# Microtubule-organizing center formation at telomeres induces meiotic telomere clustering

Masashi Yoshida,[1] Satoshi Katsuyama,[1] Kazuki Tateho,[1] Hiroto Nakamura,[1] Junpei Miyoshi,[1] Tatsunori Ohba,[1] Hirotada Matsuhara,[2] Futaba Miki,[3] Koei Okazaki,[3] Tokuko Haraguchi,[4,5] Osami Niwa,[3] Yasushi Hiraoka,[4,5] and Ayumu Yamamoto[1,2]

[1]Department of Chemistry and [2]Graduate School of Science and Technology, Shizuoka University, Suruga-ku, Shizuoka 422-8529, Japan
[3]Kazusa DNA Research Institute, Kisarazu, Chiba 292-0818, Japan
[4]Advanced Information and Communications Technology Research Institute Kobe, Nishi-ku, Kobe 651-2492, Japan
[5]Graduate School of Frontier Biosciences, Osaka University, Suita, Osaka 565-0871, Japan

During meiosis, telomeres cluster and promote homologous chromosome pairing. Telomere clustering requires the interaction of telomeres with the nuclear membrane proteins SUN (Sad1/UNC-84) and KASH (Klarsicht/ANC-1/Syne homology). The mechanism by which telomeres gather remains elusive. In this paper, we show that telomere clustering in fission yeast depends on microtubules and the microtubule motors, cytoplasmic dynein, and kinesins. Furthermore, the γ-tubulin complex (γ-TuC) is recruited to SUN- and KASH-localized telomeres to form a novel microtubule-organizing center that we termed the "telocentrosome." Telocentrosome formation depends on the γ-TuC regulator Mto1 and on the KASH protein Kms1, and depletion of either Mto1 or Kms1 caused severe telomere clustering defects. In addition, the dynein light chain (DLC) contributes to telocentrosome formation, and simultaneous depletion of DLC and dynein also caused severe clustering defects. Thus, the telocentrosome is essential for telomere clustering. We propose that telomere-localized SUN and KASH induce telocentrosome formation and that subsequent microtubule motor-dependent aggregation of telocentrosomes via the telocentrosome-nucleated microtubules causes telomere clustering.

## Introduction

In sexual reproduction, eukaryotic organisms produce haploid gametes through a type of cell division called meiosis. During meiosis, telomeres cluster and promote homologous chromosome pairing, and the paired chromosomes recombine and then segregate (Scherthan, 2001). In many organisms, telomere clustering requires the telomeres to interact with a complex composed of the SUN and KASH nuclear membrane proteins (Hiraoka and Dernburg, 2009; Razafsky and Hodzic, 2009). SUN proteins interact with telomeres, whereas KASH proteins interact with cytoskeletal elements such as cytoplasmic microtubules or actin filaments, linking the telomeres with the cytoskeleton. Cytoskeleton-dependent forces gather the telomeres by as yet unknown mechanisms.

In the fission yeast *Schizosaccharomyces pombe*, telomeres cluster at the spindle pole body (SPB; a fungal centrosome) upon entering meiosis and remain clustered until the first division (Chikashige et al., 1994). During the period of telomere clustering, the nucleus oscillates between the cell ends, pulled by the SPB. The resultant telomere-led chromosome movements facilitate homologous chromosome pairing (Chikashige et al., 1994; Yamamoto et al., 1999; Ding et al., 2004). Telomere clustering requires telomeric localization of Sad1, an SPB component that belongs to the SUN family of nuclear membrane proteins, and telomere recruitment of Sad1 depends on the meiosis-specific factors Bqt1 and Bqt2 (Chikashige et al., 2006). However, forced telomere recruitment of Sad1 by Bqt1 and Bqt2 fails to induce telomere clustering during mitosis, and the mechanism by which the Sad1-localized telomeres move and gather at the SPB remains unknown.

Correspondence to Ayumu Yamamoto: sayamam@ipc.shizuoka.ac.jp

Abbreviations used in this paper: CCD, charge-coupled device; DHC, dynein heavy chain; DLC, dynein light chain; EMM, Edinburgh minimal medium; γ-TuC, γ-tubulin complex; MBC, methyl 2-benzimidazole carbamate; ME, malt extract; MTOC, microtubule-organizing center; SPB, spindle pole body; YES, yeast extract medium with supplements.



The Rockefeller University Press $30.00
J. Cell Biol. Vol. 200 No. 4 385–395
www.jcb.org/cgi/doi/10.1083/jcb.201207168

Cytoplasmic dynein, a protein complex that moves along microtubules by ATP hydrolysis, has been suggested to contribute to telomere clustering. Cytoplasmic dynein drives nuclear oscillation, and the loss of either its motor subunit (dynein heavy chain [DHC]) or its regulatory subunit (Tctex-1–type dynein light chain [DLC]) compromises nuclear oscillation and impairs homologous chromosome pairing (Yamamoto et al., 1999; Miki et al., 2002). However, loss of both subunits reduces homologous recombination more severely than the single loss of either subunit and impairs spatial connection of the telomere-adjacent ribosomal DNA loci with the SPB during the telomere clustering stage (Miki et al., 2002). These data imply that loss of both subunits compromises telomere clustering and impairs homologous chromosome pairing more than the single losses.

Here, we show that telomere clustering in *S. pombe* depends on cytoplasmic dynein. We also show that telomere clustering depends on different types of microtubule motors, kinesins, and microtubules. Furthermore, a novel, meiosis-specific microtubule-organizing center (MTOC) is formed at the telomere, which we term the "telocentrosome." This telocentrosome plays a pivotal role in telomere clustering. Based on our findings, we propose a telocentrosome-dependent mechanism for telomere clustering that explains how cytoskeleton-dependent forces gather telomeres.

## Results and discussion

To investigate the telomere-clustering mechanism, we examined the involvement of cytoplasmic dynein in this process. *S. pombe* cells normally proliferate in the haploid state. Upon nitrogen starvation, cells of opposite mating types fuse to form a diploid zygote that enters meiosis (zygotic meiosis; Fig. 1 A). Visualization of the telomere-binding protein Taz1 (Cooper et al., 1997) and the SPB component Sid4 (Tomlin et al., 2002) showed that most nuclei contained a single telomere signal adjacent to the SPB signal in wild-type zygotes, both before and after nuclear fusion, confirming telomere clustering at the SPB (Fig. 1, B and C; and Fig. S1, A and B). Likewise, most (but not all) nuclei in *dhc1Δ* or *dlc1Δ* single mutant zygotes contained a single telomere signal. In contrast, many nuclei in *dhc1Δ dlc1Δ* double mutant zygotes contained multiple telomere signals and a single SPB signal (Fig. 1, B and C; and Fig. S1, A and B). These findings confirmed severe telomere clustering defects in the double mutant and indicate that DHC and DLC play independent crucial roles in telomere clustering. There was also an increase in clustering defects upon loss of Ssm4, a $p150^{Glued}$ subunit of dynactin (Niccoli et al., 2004), in the *dhc1Δ* background (Fig. 1 C and Fig. S1 B). This indicated that the dynactin complex, which interacts with dynein to aid its functions (Schroer, 2004), also contributes to telomere clustering.

The occurrence of telomere clustering in cells lacking dynein suggested that other microtubule motors contribute to telomere clustering. We next investigated the involvement of the microtubule motor kinesin. Depletion or impairment of kinesin motors belonging to the kinesin-5 (Cut7), -7 (Tea2), -8 (Klp5 and Klp6), or -14 (Pkl1 and Klp2) families (Steinberg, 2007) increased clustering defects in *dhc1Δ* cells, although to a lesser extent than with DLC depletion (Fig. 1 D and Fig. S1, B and C). Thus, these kinesins contribute to telomere clustering in a DHC-independent manner. They may function in the same pathway as DLC and/or play marginal roles because the clustering defects were not increased significantly by kinesin depletion or impairment in the *dlc1Δ* mutant (Fig. S1 C). Collectively, these results indicate that multiple microtubule motors contribute to telomere clustering.

Because most of the investigated motors are localized on microtubules (Fig. S1 D; Yamamoto et al., 1999; Miki et al., 2002; Niccoli et al., 2004), we examined the dynamics of telomeres with respect to microtubules. In cells undergoing conjugation, telomeres moved with microtubules and form a cluster (Fig. 2 A and Video 1). This observation suggests that telomeres gather via microtubules. To prove the microtubule dependency, we next used the microtubule inhibitor methyl 2-benzimidazole carbamate (MBC). To eliminate microtubules before telomere clustering, we induced meiosis synchronously in haploid cells bearing both mating type genes (Fig. 2 B; Yamamoto and Hiraoka, 2003). Under nitrogen-depleted conditions, these haploid cells underwent a single mitotic division to enter G1 phase and subsequently underwent meiosis without cell conjugation in a fairly synchronous manner (Fig. 2, B and C). MBC or its solvent, DMSO, was added to the medium after mitotic nuclear division. In the presence of DMSO, most telomeres formed a single cluster at the SPB after mitotic division (Fig. 2 C). In the presence of MBC, meiosis proceeded because of incomplete microtubule inhibition (as shown by the occurrence of meiotic divisions); however, most telomeres failed to form a single cluster and only partially clustered at the SPB (Fig. 2 C). These results indicate that telomere clustering depends on microtubules.

To understand the telomere–microtubule interaction and the clustering process, we allowed haploid meiotic cells to reform the microtubules after MBC treatment and examined the dynamics of telomeres and microtubules in detail. After MBC removal, cytoplasmic microtubules extended from the vicinity of telomeres, indicating MTOC formation at the telomeres (Fig. 2 D; Fig. S2, A and B; Video 2; and Video 3). The telomeric MTOC is meiosis-specific, as telomere microtubule nucleation and stable telomere–microtubule interaction were never observed during mitosis (Fig. S2 C and Video 4). We called this unusual, meiosis-specific telomeric MTOC the "telocentrosome." The telomeres drifted inside the cell with the telocentrosome-nucleated microtubules (Fig. 2 D, 0–344 s) and gathered once they were connected by the microtubules (Fig. 2 D, 367–456 s). These observations show that telomeres gather via telocentrosomal microtubules. Notably, the telomeres have minus end–directed motile activity, as shown by movement on the microtubule toward the nucleation site upon microtubule interaction (Fig. 2 E, arrows; and Video 5). The telocentrosome is also formed during zygotic meiosis. Before cell conjugation, telomeres often partially clustered at the SPB, and Sad1 became localized at the nonclustering telomeres (Sad1-Taz1 colocalization was observed in 90.3% of cells containing multiple Sad1 dots [$n$ = 73]; Fig. 3 A).

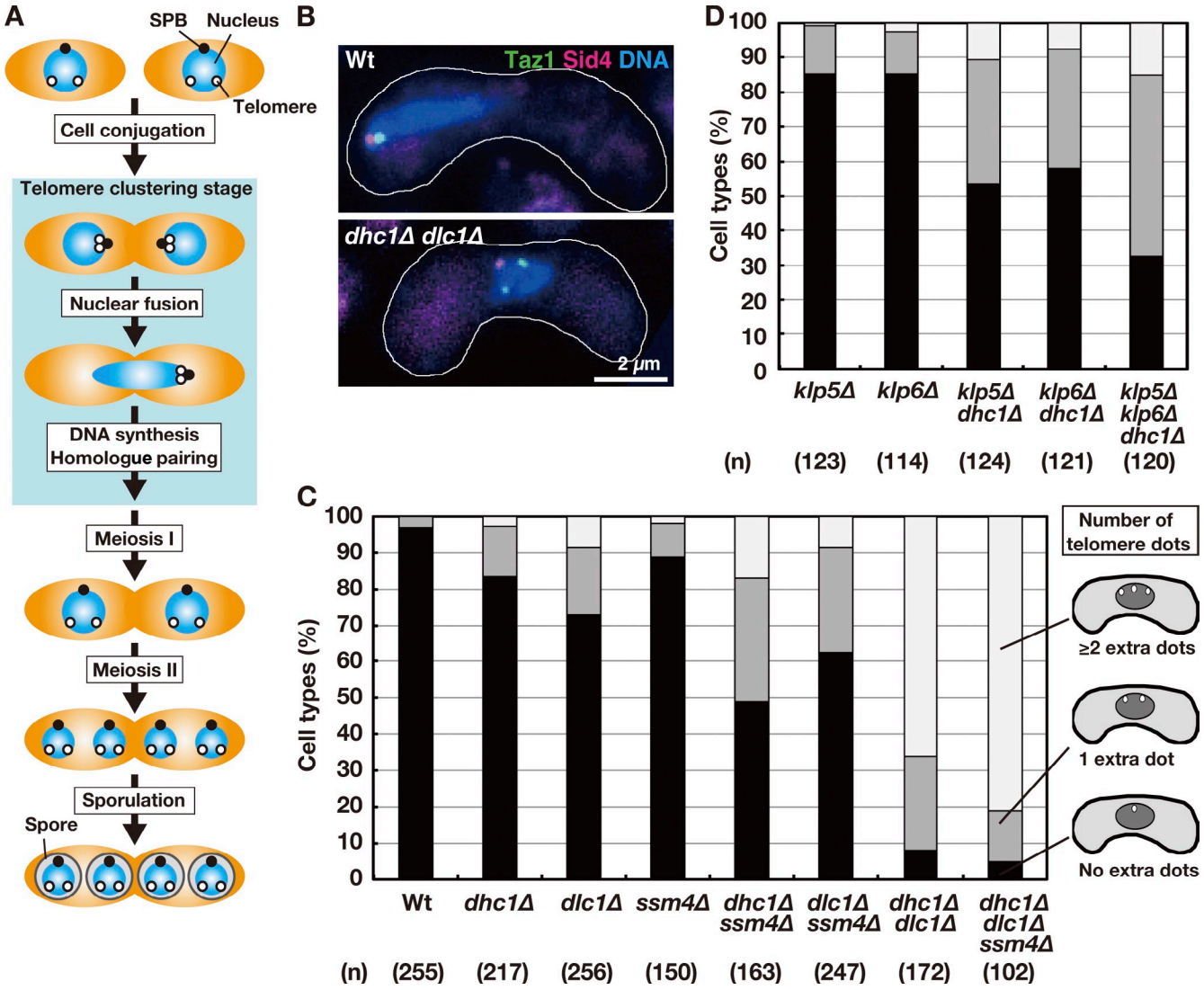


Figure 1. **Telomere clustering defects in dynein and kinesin-8 mutants.** (A) The meiotic process in fission yeast. (B) Telomere and SPB locations in wild-type (Wt) and *dhc1Δ dlc1Δ* mutant zygotes with a single nucleus. White lines indicate cell shapes. (C and D) Telomere distribution in dynein, dynactin, and kinesin-8 mutant zygotes with a single nucleus.

The telocentrosomes formed at the Sad1-localized telomeres, as shown by microtubule nucleation from the Sad1 dots after MBC treatment (Fig. S2 D and Video 6).

To investigate telocentrosome formation, we looked at telocentrosome-localized factors before cell conjugation. Because of the MTOC activity, we examined SPB components by analyzing their colocalization with multiple Sad1 dots that corresponded to the telocentrosomes and the SPB. The SPB-localized KASH proteins Kms1 and Kms2 (Starr and Fischer, 2005) can interact with Sad1 and/or are required for telomere clustering (Shimanuki et al., 1997; Miki et al., 2004). Kms1 and Kms2 colocalized with the telocentrosome, as shown by colocalization with multiple Sad1 dots (Fig. 3, A and B). Dhc1, Dlc1, and Ssm4 also colocalized with the telocentrosome (Fig. 3, A and C). Furthermore, Alp4, an essential component of the γ-tubulin complex (γ-TuC) that induces microtubule nucleation (Vardy and Toda, 2000), and its regulator, Mto1 (Sawin et al., 2004; Venkatram et al., 2004), colocalized with the telocentrosome (Fig. 3, A and D). Unlike these SPB components, however, Sid4 did not colocalize (Fig. 3, A and D). Thus, a subset of SPB components localized to the telocentrosome.

We next examined the interdependence of telocentrosomal factor localization. Telomere localization of Dhc1 and Dlc1 was mutually independent, and Ssm4 localization to the telomere and the SPB was Dhc1 dependent (Fig. 3 C and Fig. S2 E). Furthermore, Dhc1 localization did not require dynein motor activity, as shown by Sad1 localization of a Dhc1 fragment lacking a motor domain (Fig. 3 E and Fig. S2 F). Dlc1 localization was Kms1 dependent (Fig. 3 C), consistent with their direct interaction (Miki et al., 2004). Importantly, Alp4 telomere localization depended substantially on Kms1 and Mto1, and Mto1 localization depended on Kms1 (Fig. 3 D). Therefore, Kms1 and Mto1 are required for telocentrosome formation, and Kms1 tethers γ-TuC to telomeres, probably via Mto1.

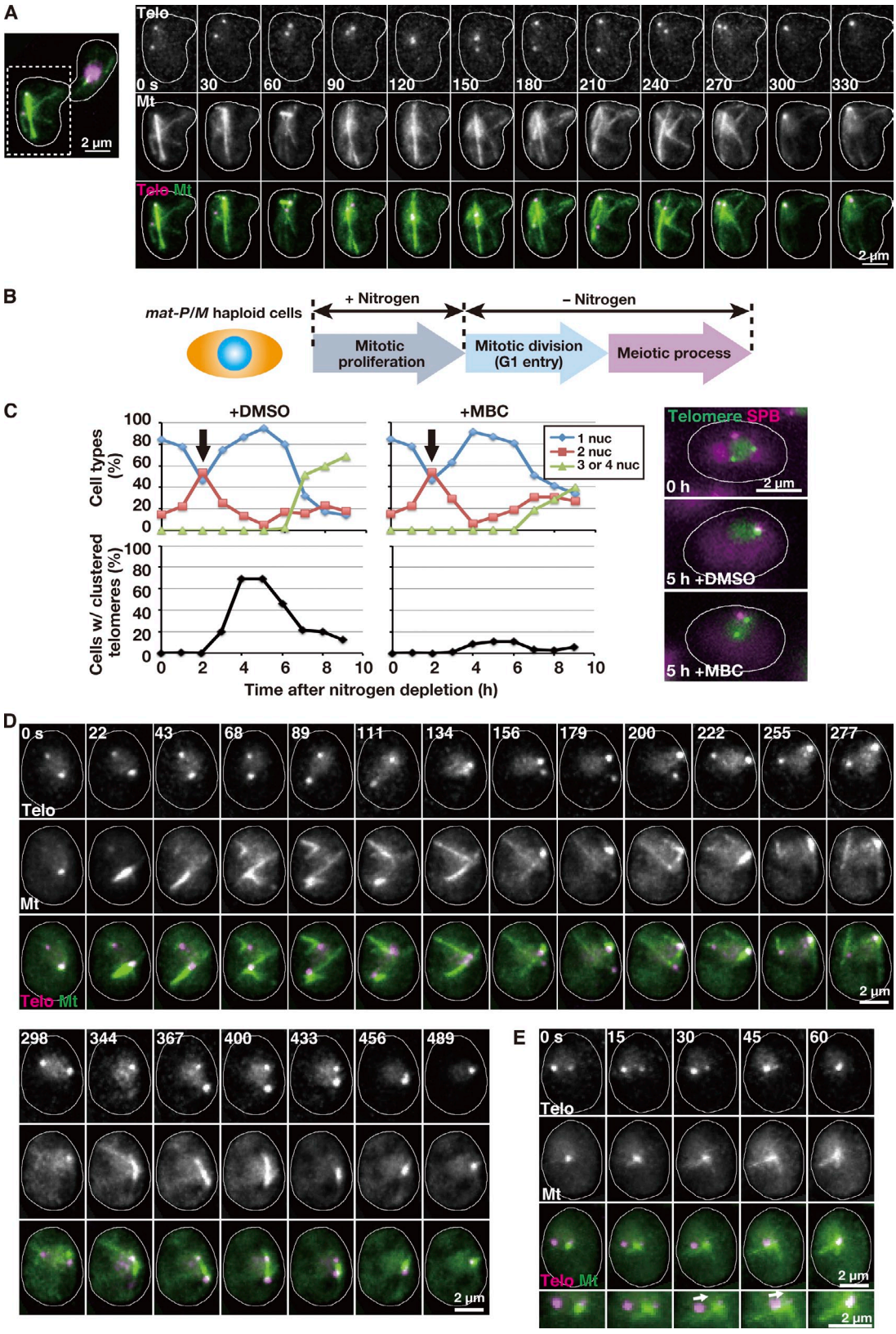


Figure 2. **Telomere clustering depends on microtubules.** (A) The dynamics of telomeres (Telo) and microtubules (Mt) before cell conjugation. A left photo shows an examined cell, which is undergoing cell conjugation (white dashed box). (B) Schematic showing *mat* gene-induced haploid meiosis. (C) Meiotic progression (top graphs) and telomere clustering (bottom graphs) in haploid meiosis. Arrows show the addition of DMSO (left) or 50 µg/ml MBC (right). The data shown are from a single representative experiment out of two repeats. More than 100 cells were examined at each time point. Photos indicate the location of telomeres (Taz1) and SPB (Sid4). nuc, nucleus. (D and E) Dynamics of microtubules and telomeres in a haploid meiotic cell after MBC removal. MBC was removed ~5 h after nitrogen depletion. In E, enlarged images are shown at the bottom row. Arrows show the telomere movement. White lines indicate cell shapes.

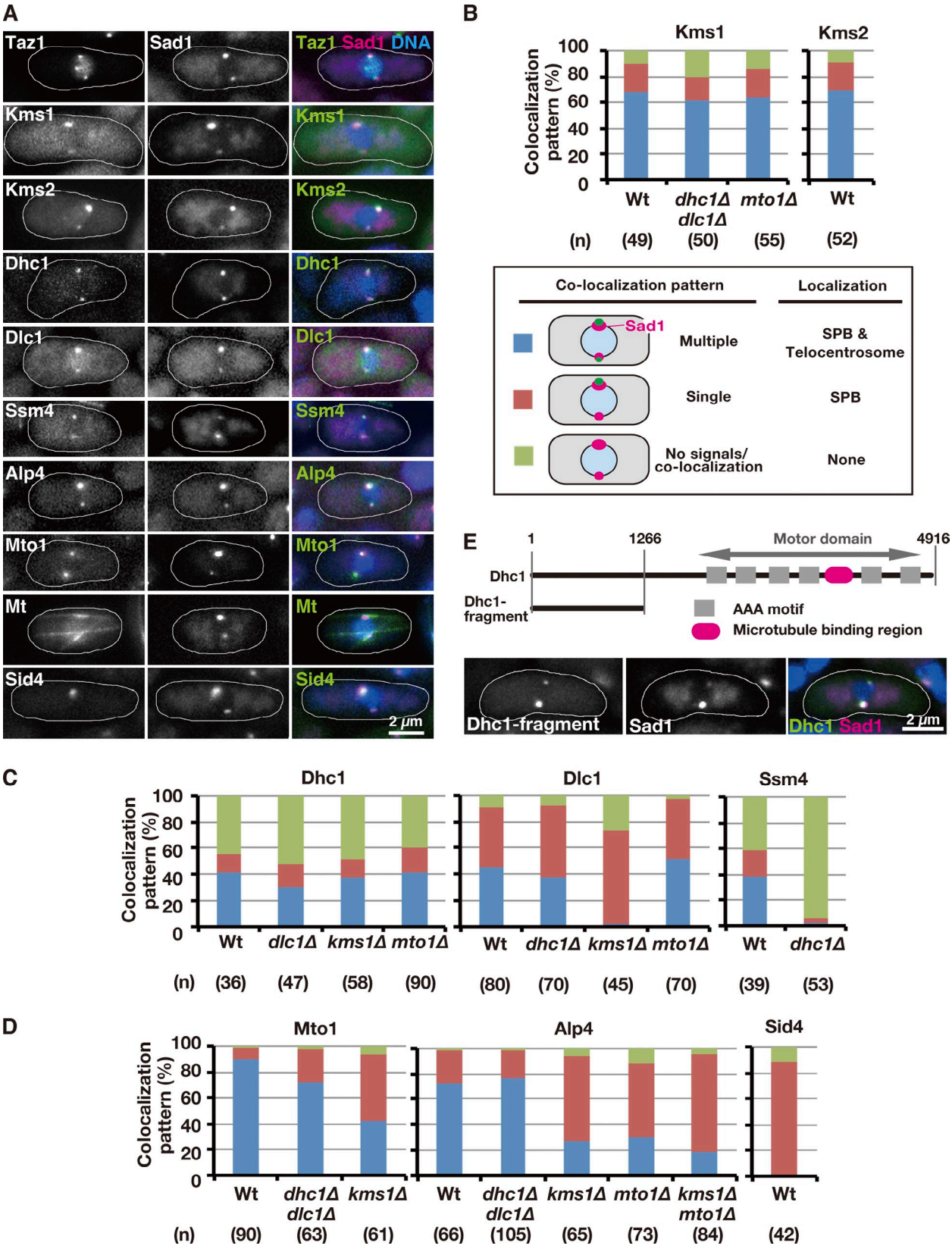


Figure 3. **Telomere-localized factors before cell conjugation.** (A) Colocalization of various factors with telomeres (Taz1) or Sad1. (B–D) Colocalization patterns of the various factors in cells containing multiple Sad1 signals before cell conjugation. (E) Intracellular localization of a Dhc1 fragment lacking a motor domain before cell conjugation. The schematic indicates the Dhc1 architecture as deduced from amino acid sequence homology (Mocz and Gibbons, 2001) and the region containing the Dhc1 fragment. Numbers indicate amino acid positions. White lines in images indicate cell shapes. Mt, microtubule; Wt, wild type.

If telomere clustering depends on the telocentrosome, telocentrosome defects should be associated with telomere clustering defects. The *kms1* mutant consistently shows severe telomere clustering defects and defective homologous chromosome pairing (Shimanuki et al., 1997; Niwa et al., 2000). The *mto1Δ* mutant also showed severe telomere clustering defects (Fig. 4, A and C) and phenotypes associated with defective pairing (reduced spore viability and meiotic recombination; Fig. 4 B). These results show that telomere clustering depends on the telocentrosome.

The telomeric localization of Dhc1 and Dlc1 raised the possibility that telomere clustering defects seen in the *dhc1Δ dlc1Δ* double mutant resulted from defective telocentrosome formation. Indeed, as seen in *mto1Δ* or *kms1Δ* zygotes, Sad1 mostly colocalized with telomeres (Fig. 4 C), but Alp4 and Mto1 were frequently absent or barely visible at the Sad1 dots in *dhc1Δ dlc1Δ* zygotes (Fig. 4, D and E). In addition, microtubules and the SPB-originated MTOC often failed to colocalize with the Sad1 dots (Fig. 4 F). Therefore, the Sad1–γ-TuC interaction appears to be reduced in the double mutant, as in *mto1Δ* and *kms1Δ* mutants. However, because strong Sad1 colocalization of Alp4 and Mto1 was observed before cell conjugation as in wild-type cells (Fig. 3 D), the interaction appears to diminish only after cell conjugation.

To evaluate the contribution of DHC and DLC to the telocentrosome, we examined Alp4 telomere localization and the effects of Dhc1 and/or Dlc1 depletion in *mat* gene-induced haploid meiosis. We inhibited telomere clustering by MBC and simultaneously visualized the SPB (Sid4) to assess Alp4 telomere localization (via Taz1; Fig. 5 A). In wild-type cells treated with MBC, Alp4 telomere localization increased along with the increase in telomere clustering (Fig. 5 B). However, Alp4 localization to the telomere was substantially reduced in telomere clustering–defective *mto1Δ* cells (Fig. 5 B) despite progression of meiosis (Fig. S3). These results confirm the validity of this assay and the importance of Mto1 in telocentrosome formation. The telomere clustering defects in dynein mutant zygotes were mirrored in haploid meiotic cells (Fig. 5 B, blue lines). Importantly, Alp4 localized to the telomeres in *dhc1Δ* cells, but Alp4 localization was dramatically reduced in *dlc1Δ* cells and in *dhc1Δ dlc1Δ* cells (Fig. 5 B). Therefore, Dlc1 contributes to γ-TuC telomere localization, but Dhc1 does not. Together with the independent telomere/SPB localization of Dhc1 and Dlc1 (Fig. 3 C and Fig. S2 E) and the retention of the Dhc1 function in *dlc1Δ* cells (Miki et al., 2002), these results indicate that the telomere clustering defects seen in the *dhc1Δ dlc1Δ* mutant arise from a combination of telocentrosome defects and loss of dynein motor activity.

Our results show that microtubule motor-dependent aggregation of telocentrosomes causes telomere clustering. Studies have shown that acentrosomal spindle poles are formed in a dynein-dependent manner in *Xenopus laevis* egg extracts and by MTOC aggregation in mouse oocytes (Heald et al., 1996; Schuh and Ellenberg, 2007). Given their similarities, the processes of telomere clustering and acentrosomal spindle pole formation likely share the same mechanism. Considering this possibility, we propose the following telomere clustering mechanism (Fig. 5 C). Upon entering meiosis, Bqt1 and Bqt2 recruit Sad1 to telomeres along with Kms1 and Kms2. This recruitment causes telomere recruitment of the γ-TuC via Mto1, forming the telocentrosome. Simultaneously, cytoplasmic dynein is recruited to the telomere in a motor-independent fashion, whereas Dlc1 is independently tethered to telomeres via Kms1 and may act to maintain the telomere γ-TuC in the later stage. Kinesin motors Pkl1 and Cut7 may also contribute to γ-TuC telomere localization despite the absence of obvious telocentrosomal localization, as they genetically and/or physically interact with γ-tubulin (Pidoux et al., 1996; Paluh et al., 2000; Rodriguez et al., 2008). Subsequently, oligomerized cytoplasmic dynein and minus end–directed kinesin-14 motors gather telomeres at the SPB by cross-linking the SPB- and telocentrosome-nucleated microtubules and by moving along these microtubules toward the nucleation sites. Telomere-tethered dynein probably also facilitates telomere clustering by direct transport of the telomere along the microtubules. Because the investigated kinesins and an Ssm4 homologue $p150^{Glued}$ are suggested or shown to regulate microtubule polymerization and/or bundling (Hagan and Yanagida, 1992; Pidoux et al., 1996; Browning et al., 2000; Troxell et al., 2001; Ligon et al., 2003; Grissom et al., 2009; Erent et al., 2012), the kinesins and Ssm4 may contribute to telomere clustering by regulating dynamics and/or cross-linking of the telocentrosomal microtubules.

In our model, the telocentrosome is essential for telomere clustering. This is supported by the observation of severe telomere clustering defects in the telocentrosome-defective *kms1Δ* and *mto1Δ* mutants. In addition, dynein is a major motor for telomere clustering. This model explains why telomere clustering was severely compromised in the *dhc1Δ dlc1Δ* double mutant but mildly affected in the *dhc1Δ* or *dlc1Δ* single mutant and the *dlc1Δ* kinesin double mutants. In the absence of dynein, distinct kinesin motors gather telomeres cooperatively. In the absence of DLC, the telocentrosome forms transiently, perhaps at an early stage, and dynein and kinesin motors gather telomeres during this period. This situation is largely unchanged by the concomitant depletion of some kinesins. However, when dynein is depleted simultaneously with DLC, kinesin motors alone fail to gather telomeres.

Our findings have several important implications. First, it is likely that our model applies to telomere clustering in other organisms. In worms, the specialized chromosomal domains called "pairing centers" aggregate to promote homologous chromosome pairing (MacQueen et al., 2005). Pairing centers interact with the SUN and KASH proteins, and their aggregation depends on microtubules and cytoplasmic dynein (Penkner et al., 2007; Sato et al., 2009). These similarities between two evolutionarily distant organisms imply that the telomere clustering mechanism is conserved among eukaryotes. Second, our finding of DLC-dependent regulation of the γ-TuC contributes to understanding of the spatiotemporal regulation of the MTOC and a recently identified link between telomere clustering and meiotic spindle formation (Tomita and Cooper, 2007). In addition, Tctex-1–type DLC regulates neurite outgrowth by interacting directly with a G protein in a dynein motor–independent manner (Sachdev et al., 2007), and our finding

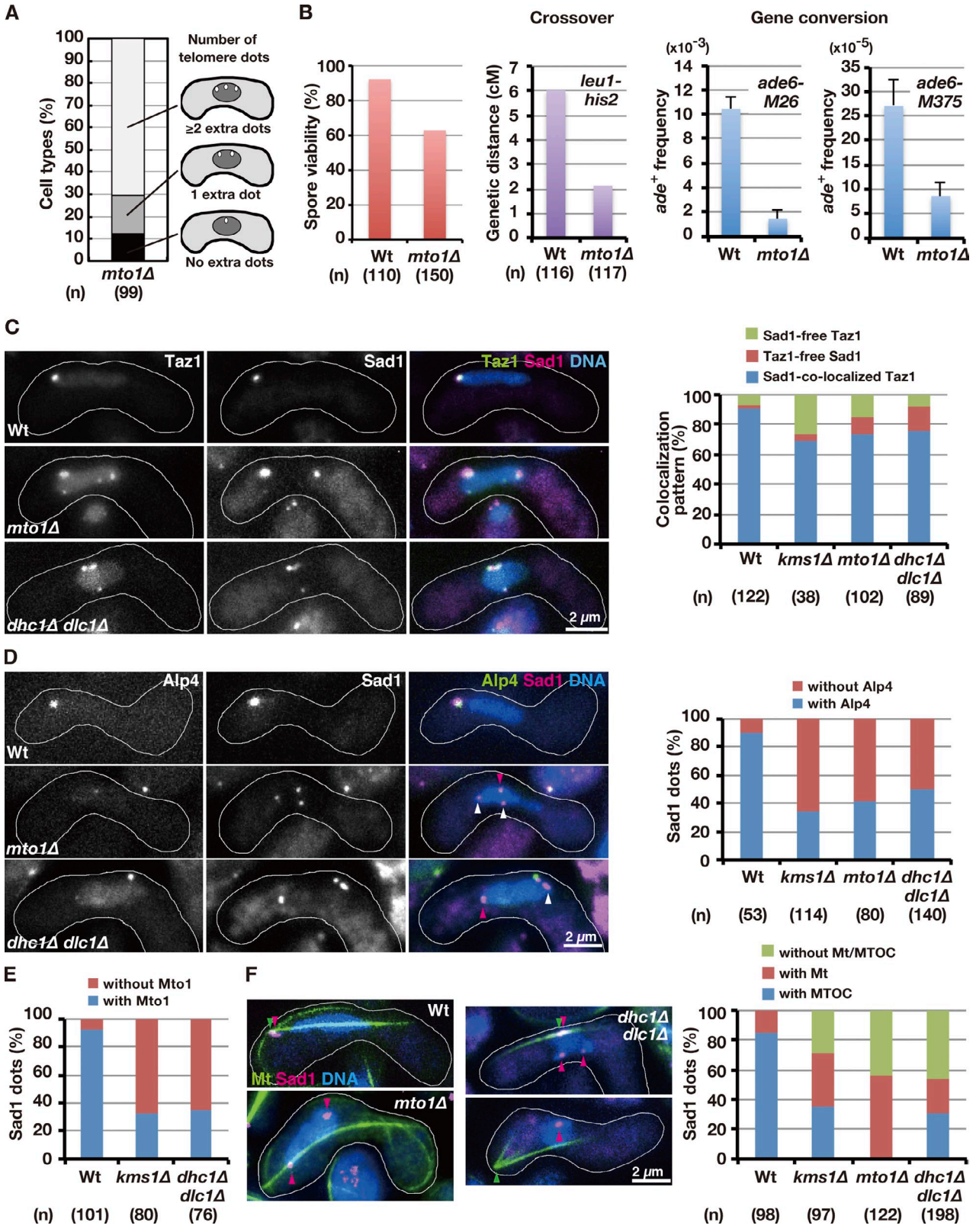


Figure 4. **Defective telomere clustering and reduced spore viability and recombination in the *mto1Δ* mutant and defective telomere interaction of Alp4 and microtubules in the *mto1Δ*, *kms1Δ*, and *dhc1Δ dlc1Δ* zygotes.** (A) Telomere clustering defects in *mto1Δ* zygotes. (B) Reduced spore viability and meiotic recombination in the *mto1Δ* mutant. *n*, number of spores or tetrads that were examined. Graphs of gene conversion show mean *ade*$^+$ frequencies. Error bars indicate SEM ($n = 3$). (C) Sad1 and telomere localization and their colocalization frequency. (D) Alp4 and Sad1 localization and their colocalization frequency. Arrowheads indicate Alp4-free (white) and -diminished (magenta) Sad1 dots. (E) Colocalization frequency of Mto1 and Sad1. (F) Microtubule organization (Mt) and Sad1 location (magenta arrowheads). Green arrowheads, SPB-originated MTOCs. An obvious MTOC was not observed in the *mto1Δ* mutant. White lines in images indicate cell shapes. Wt, wild type.

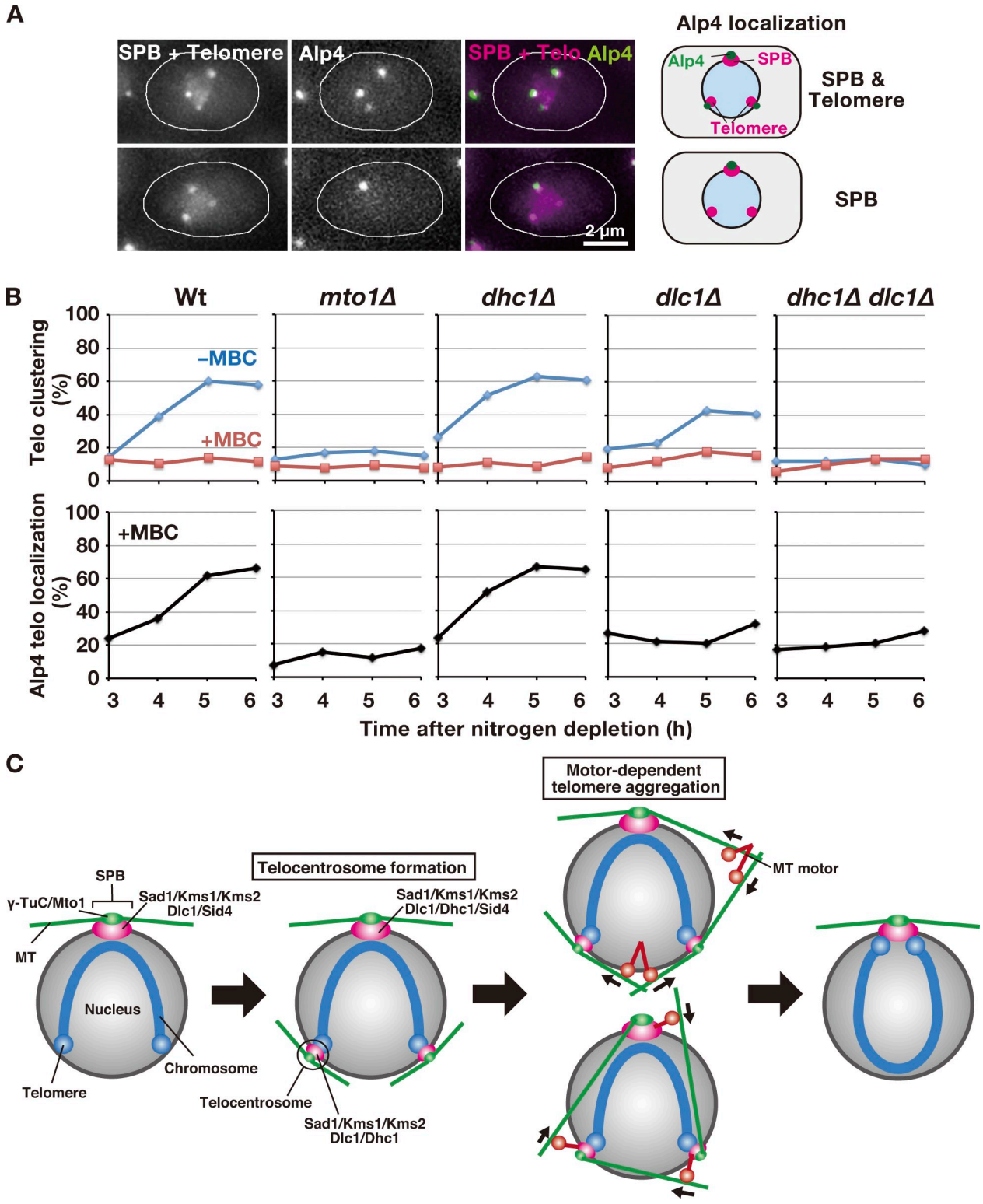


Figure 5. **Defective Alp4 telomere localization in haploid *mto1Δ* and *dlc1Δ* mutants and the telomere clustering mechanism.** (A) Representative Alp4 localization in relation to telomeres (Taz1) and the SPB (Sid4). White lines indicate cell shapes. (B) Telomere (Telo) clustering in haploid meiotic cells (top graphs) and Alp4 telomere localization in MBC-treated cells (bottom graphs). The experiment of *mto1Δ* mutant was completed once. The data of other strains are from a single experiment out of two (wild type [Wt] and *dhc1Δ*) or three (*dlc1Δ* and *dhc1Δ dlc1Δ*) repeats. More than 100 cells were examined at each time point. (C) A proposed model for the telomere clustering mechanism. MT, microtubule.

sheds light on the dynein motor–independent functions of Tctex-1–type DLC. Finally, because telomere clustering defects cause improper homologous chromosome pairing and thus defective homologous chromosome segregation, our findings may shed light on the mechanisms underlying birth-associated chromosome missegregation that lead to a miscarriage or Down's syndrome.

## Materials and methods

### Strains and media

The strains used in this study are shown in Table S1. Yeast extract medium with supplements (YES) or Edinburgh minimal medium (EMM) was used for vegetative growth, whereas malt extract (ME) medium or EMM medium lacking ammonium chloride (EMM-N) was used for the induction of meiosis (Moreno et al., 1991).

### Plasmid construction for visualizing intracellular structures or molecules and introduction of the plasmids into cells

**Telomere visualization.** To visualize telomeres, we constructed a plasmid, pMY23, encoding an *mCherry* and *taz1*$^+$ fusion as follows: An *ars1*-coding region was removed from pAUR224 (Takara Bio Inc.) by digesting pAUR224 with MluI and AflII and self-ligating it after blunting the digested DNA ends with a Klenow fragment. A critical portion of the cytomegalovirus promoter was removed from the resulting plasmid by digesting the plasmid with NcoI and XhoI and then self-ligating it after blunting the digested DNA ends with a Klenow fragment. This resulted in pTO2. The *mCherry* (Shaner et al., 2004) coding region was excised from an *mCherry*-bearing plasmid (a gift from K. Tanaka, University of Leicester, Leicester, England, UK) with BamHI and MluI and inserted in the corresponding sites of pTO2, producing pHM4. Finally, a DNA region encoding the *taz1*$^+$ promoter and ORF was amplified by PCR using two synthetic oligonucleotide primers, 5′-CCGCTCGAGCATCGACAAGGCATGCGAAGCT-3′ and 5′-GCGGATCCTAGATTGATAATTAACAAGCTCTTCC-3′, and fission yeast genomic DNA as a template. The amplified DNA fragment was digested with BamHI and XhoI and inserted in the BamHI and SalI sites of pHM4. The resulting plasmid, pMY23, was transformed into cells, and integrants were selected by resistance to the antibiotic aureobasidin A (Takara Bio Inc.).

Alternatively, we generated C-terminal mCherry-tagged Taz1 by the two-step PCR-based method (Krawchuk and Wahls, 1999). We first constructed an *mCherry* module plasmid (pHM22) by inserting the *mCherry*-encoding DNA region of the *mCherry*-bearing plasmid between the SalI and BglII sites of pFA6a-*nat*MX6 (obtained from T. Carr, University of Sussex, Sussex, England, UK; Hentges et al., 2005). We amplified DNA fragments encoding the Taz1 C terminus–coding region or the *taz1*$^+$ terminator by PCR using two sets of synthetic oligonucleotide primers (5′-CTGGTGGTAGAAGTTCGGCAA-3′ and 5′-CCTTAATTAACCCGGGGATCCGAGATTGATAATTAACAAGCTCTTCC-3′; and 5′-TTTTCGCCTCGACATCATCTTTTTTCGTCTCCGGATAGAGTTT-3′ and 5′-CGCAATTTGGGATTGAAAACCTA-3′) and genomic DNA as a template. We then amplified the *mCherry* module by PCR using the two PCR products as primers and pHM22 as a template. The resulting PCR product was introduced into cells, and integrants were selected by resistance to the antibiotic nourseothricin (WERNER BioAgents) and confirmed by PCR and microscopic observation.

**Microtubule visualization.** To visualize microtubules, we constructed plasmids pMY53 and pMY56, which encoded an *mCherry* and *atb2*$^+$ fusion gene as follows: A coding region of the *nda3* promoter in a plasmid containing the *mDsRed* and *atb2*$^+$ fusion gene (Yamamoto et al., 2008) was removed to create a BamHI site at the removal site using two synthetic oligonucleotide primers, 5′-CTAGACTAATTTATGGTGGTTTGTTTTG-3′ and 5′-GGATCCATGAGAGAGATCATTTCCATTCACGTT-3′, following the instructions for the KOD-Plus-Mutagenesis kit (Toyobo Co., Ltd.). A DNA fragment encoding *mCherry* was amplified by PCR using two synthetic oligonucleotide primers, 5′-TCAGATCTCTTGTACAGCTCGTCCATGCC-3′ and 5′-GGGGGCGAGCTCAGATCTATGGTGAGCAAGGGCGAGGA-3′, and the *mCherry*-bearing plasmid as a template. The amplified DNA fragment was digested with BglII and inserted at the BamHI site of the *atb2*$^+$ gene-bearing plasmid to yield the *mCherry-atb2*$^+$ integration plasmid pMY53. For constructing pMY56, the *mCherry-atb2*$^+$ fusion gene along with the *nda3* promoter was amplified by PCR using two synthetic oligonucleotides, 5′-CAGGAAACAGCTATGACCATGA-3′ and 5′-CGGGATCCCTATAGGGCGAATTGGAGCTC-3′, and pMY53 as a template. The amplified DNA fragment was digested with XhoI and BamHI and inserted between the SalI and BamHI sites of pTO2 to yield pMY56. To construct strains expressing the *mCherry-atb2*$^+$ fusion gene, pMY53 or pMY56 was transformed into *lys1-131* or aureobasidin A–sensitive cells, respectively. The integrants were selected by the *lys*$^+$ or *aur*$^r$ phenotype and further confirmed by microscopic observation.

**Kms2 visualization.** To visualize Kms2, we constructed plasmid pMY16, which encoded a *GFP* and *kms2*$^+$ fusion gene as follows: A DNA fragment coding for *GFP* was amplified by PCR using two synthetic oligonucleotides, 5′-CCGCTCGAGATCTATGTCTTTAATTAACAGTAAAGGAG-3′ and 5′-CCGCTCGAGGGATCCTTTGTATAGTTCATCCATGCCAT-3′, and pFA6a-GFP(S65T)-kanMX6 (Bähler et al., 1998) as a template. The amplified DNA fragment was digested by XhoI and inserted at the SalI site of pYC36 (obtained from Y. Chikashige, Advanced Information and Communications Technology Research Center, Kobe, Japan; Chikashige et al., 2004) to produce pMY12. A DNA fragment encoding the *kms2*$^+$ promoter was amplified by PCR using two synthetic oligonucleotide primers, 5′-CGGGATCCTTTGATTGTTTATTGACATGTGCT-3′ and 5′-CGGGATCCGAGAAGTAGGAGATATAATCGTC-3′, and fission yeast genomic DNA as a template. The fragment was inserted at the BglII site of pMY12 after digestion with BamHI. Subsequently, a Kms2-coding region and its terminator were amplified by PCR using two synthetic oligonucleotide primers, 5′-GAAGATCTATGGATGAATACATCCCTTTTGA-3′ and 5′-GAAGATCTAGTTATAAAAGAGAAATTATGAGAAA-3′, and fission yeast genomic DNA as a template. The amplified gene was then inserted in frame after the *GFP* gene in the constructed plasmid by inserting the fragment at the BamHI site after BglII digestion. The resulting plasmid, pMY16, was introduced into cells as described for pMY53.

**Dlc1 visualization.** To visualize Dlc1, we constructed a plasmid, pMY21, encoding the *dlc1*$^+$ and *GFP* fusion gene as follows: A DNA fragment coding *GFP* with the *Saccharomyces cerevisiae ADH1* terminator was amplified by PCR using two synthetic oligonucleotides, 5′-ACGCGTCGACGAAGATCTTCGGATCCCCGGGTTAATTAAC-3′ and 5′-GGGGTACCATATTACCCTGTTATCCCTAGCG-3′, and pFA6a-GFP(S65T)-kanMX6 as a template. The amplified DNA fragment was digested with SalI and KpnI and inserted between the corresponding sites of pYC36 to yield pTO7. Subsequently, a DNA fragment encoding the *dlc1*$^+$ promoter and ORF was amplified by PCR using two synthetic oligonucleotides, 5′-ACGCGTCGACTAAAGATTTGGATGATTTCGCTAC-3′ and 5′-GAAGATCTATAATGGGAGATCCACATAATGCTC-3′, and fission yeast genomic DNA as a template. The fragment was then digested with BglII and SalI and inserted between the corresponding sites of pTO7 to yield pMY21. pMY21 was introduced into cells as described for pMY53.

**Tea2 visualization.** To visualize Tea2, we constructed a plasmid, pMY36, encoding a *tea2*$^+$ and *GFP* fusion gene as follows: A DNA fragment encoding the promoter and ORF of the *tea2*$^+$ gene was amplified by PCR using two synthetic oligonucleotides, 5′-AAACTGCAGACGAAAGCCAGCTACCTGTTG-3′ and 5′-CGCGGATCCAAAGAAAGAAGTTGCGTTTCCTGAG-3′, and fission yeast genome DNA as a template. The fragment was then digested with PstI and BamHI and inserted between the PstI and BglII sites of pTO7 to yield pMY36. pMY36 was introduced into cells as described for pMY53.

**SPB visualization.** To visualize the SPB, we constructed a plasmid, pMY2, that encoded the *mRFP* and *sid4*$^+$ fusion gene as follows: Using an epitope-tagging cassette (Sato et al., 2005), the *mRFP* gene together with the *TEF* terminator was integrated into the yeast chromosome so that the *mRFP* ORF was fused in frame with the *sid4* ORF at the Sid4 C terminus. For alternative visualization, a DNA fragment encoding the *sid4*$^+$*-mRFP* fusion gene together with its promoter and terminator was amplified by PCR using two synthetic oligonucleotide primers, 5′-CCGCTCGAGCGTTAAAGCTCAATGATCAATCTT-3′ and 5′-CCGGCGGGGACGAGGCAA-3′, and genomic DNA from cells containing the *sid4*$^+$*-mRFP* fusion gene as a template. The fragment was digested with BglII and XhoI and inserted between the BamHI and SalI sites of pTO2. The resulting plasmid, pMY2, was introduced into cells as described for pMY53.

**Nuclear membrane visualization.** To visualize the nuclear membrane, we generated C-terminal mCherry-tagged Cut11 (West et al., 1998) by the two-step PCR-based method, as described for telomere zvisualization. We used two sets of synthetic oligonucleotide primers (5′-CTACAACCCCGGTTAATGAAGG-3′ and 5′-CCTTAATTAACCCGGGGATCCGGGAGTTGCTTTTGTATTCTCGAA-3′; and 5′-TTTTCGCCTCGACATCATCTGTCATCCTATAAGGTAGGTTTGT-3′ and 5′-CAAGGATCTTAAACCTCTTGGG-3′) and pHM22 as a module plasmid.

### Analysis of telomere clustering in zygotic meiosis

Cells grown on YES solid medium at 30°C were transferred to ME solid medium and induced to enter meiosis by incubation at 25°C for 16–18 h. Nuclear DNA in meiotic zygotes was stained with DNA-specific Hoechst 33342 dye (Invitrogen) by incubating the zygotes in distilled water containing 5 µg/ml Hoechst 33342 for 5 min. Telomeres visualized using GFP-tagged Taz1 were observed using an epifluorescence microscope (IX51; Olympus) or a fluorescence microscope (IX71; Olympus) equipped with a 60×/1.42 NA or 100×/1.40 NA Plan Apochromat oil immersion objective lens and a charge-coupled device (CCD) camera (DP30BW; Olympus). All images were analyzed by MetaView or MetaMorph software (Molecular Devices).

### Synchronous induction of meiosis in haploid cells and disruption of microtubules

Haploid cells bearing both types of the mating type genes were constructed by integrating the *mat-P* gene at the *lys1*$^+$ or the *aur1*$^+$ locus of *h*$^-$ haploid cells. The *mat-P* gene was integrated at the *lys1*$^+$ locus using the *mat-P* integration plasmid (pAY153) as described previously (Yamamoto and Hiraoka, 2003). For *mat-P* integration at the *aur1*$^+$ locus, we constructed an integration plasmid, pKT3, by amplifying a DNA fragment encoding the *mat-P* gene and inserting it at the SalI site of pTO2. The *mat-P* gene was integrated at the *aur1*$^+$ locus as described for pAY153, except that the integrants were selected by a resistant phenotype to the antibiotic aureobasidin A.

Haploid cells bearing both types of the mating type genes were grown to the early stationary phase in YES medium at 30°C and transferred to EMM-N medium. Cells were induced to enter meiosis by incubation at 30°C with vigorous shaking. To monitor meiotic progression, a portion of the cell culture was removed every hour, and the chromosomal morphology of the cells was analyzed by staining DNA in 0.1 M Tris-Cl, pH 9.0, containing 1 µg/ml DAPI. To disrupt microtubules, 1/200 volume of 10-mg/ml MBC (Sigma-Aldrich) in DMSO was added to the culture medium. For the control experiment, the same amount of DMSO without MBC was added instead.

### Live-cell analysis of telomere and microtubule dynamics

To follow dynamics of telomeres and microtubules in normal zygotic meiosis, cells expressing mCherry-tagged Taz1 and GFP-tagged Atb2 were induced to enter meiosis on the solid ME medium, as described for telomere clustering analysis. The cells were suspended in EMM-N medium, and a total of 20 µl of the cell suspension was placed on a 35-mm glass-bottomed culture dish (Matsunami Glass Ind., Ltd.) precoated with *Bandeiraea simplicifolia* lectin (Sigma-Aldrich). To follow telomere and microtubule dynamics in haploid meiotic cells, cells expressing mCherry-tagged Taz1 and GFP-tagged Atb2 or those expressing GFP-tagged Taz1, mCherry-tagged Atb2, and RFP-tagged Sid4 were induced to enter meiosis synchronously and treated with MBC as described for the analysis of haploid meiotic cells. A total of 30 µl of the MBC-containing cell suspension was placed on a 24 × 60–mm coverslip (Matsunami Glass Ind., Ltd.) precoated with lectin. After the cells were immobilized on the surface of the coverslip, the MBC-containing EMM-N medium was removed using a micropipette, and 100 µl MBC-free EMM-N medium was immediately placed on the coverslip to allow the cells to reform microtubules. Cells were kept at 25–27°C during live-cell observation.

GFP and RFP images of the cells at seven focal planes spaced at 0.5-µm intervals were taken through a 60×/1.42 NA Plan Apochromat oil immersion objective lens using a fluorescence microscope (IX71) equipped with a cooled CCD camera (CoolSNAP-HQ2; Nippon Roper Co. Ltd.) and controlled by MetaMorph software. The images taken at each time point were processed by deconvolution and combined to form a 2D projection in MetaMorph software.

### Construction of strains expressing a fusion of a Dhc1 fragment lacking a motor domain and GFP

The gene encoding GFP was amplified by PCR using two synthetic oligonucleotide primers, 5′-CGCGGATCCATGAGTAAAGGAGAAGAACTT-3′ and 5′-GAAGGCCTATTTGTATAGTTCATCCATGCC-3′, and digested with BamHI and StuI. It was then fused with the *nmt1* terminator by inserting it between the BamHI and SmaI sites of the pREP1 plasmid (Maundrell, 1993). A DNA fragment encoding GFP and the *nmt1* terminator was excised from the resulting plasmid by digestion with BamHI and SacI and inserted between the corresponding sites of the pRS405 plasmid bearing the *S. cerevisiae LEU2* gene (Sikorski and Hieter, 1989) to produce pAY147. A DNA fragment encoding a portion of the *dhc1*$^+$ ORF was amplified by PCR using two synthetic oligonucleotide primers, 5′-AGAGATTCCTGCTTCAGG-3′ and 5′-GAAGATCTACTTGAAGCACACCATTCAGA-3′, and pDHC1-Cla (Yamamoto et al., 1999) as a template. The PCR product was digested with EcoRV and BglII and inserted between the BamHI and SmaI sites of pAY147 to generate a fusion gene that encoded part of the *dhc1*$^+$ ORF and the GFP ORF. The resulting plasmid, pAY182, was integrated at the *dhc1*$^+$ locus by transforming it into fission yeast cells bearing the *leu1-32* mutation. When integrated at the *dhc1*$^+$ locus by homologous recombination, the *GFP* gene was fused to the *dhc1*$^+$ gene so that an N-terminal portion of Dhc1 that lacked the motor domain was tagged with GFP. The integrants were selected by the *leu*$^+$ phenotype and confirmed by Southern blot analysis.

### Analysis of spore viability and meiotic recombination

For spore viability analysis, cells were grown on solid YES medium at 30°C and induced to enter meiosis on ME solid medium at 25°C. The spores were dissected randomly under a microscope (BX40; Olympus), and their viability was determined by colony formation on the YES solid medium. To determine the recombination frequency, two strains bearing appropriate genetic markers were induced to enter meiosis as for the spore viability analysis. Crossover recombination was examined by tetrad analysis. Gene conversion at the *ade6* locus was examined as described previously (Ponticelli and Smith, 1989) except that the spore suspension was heated at 55°C for 30 min after glusulase treatment to eliminate vegetative cells.

### Online supplemental material

Fig. S1 shows telomere clustering defects in dynein and kinesin mutants and the intracellular localization of kinesin motors. Fig. S2 shows microtubule and telomere dynamics and Sad1 localization of Dhc1 and Dlc1. Fig. S3 shows meiotic progression in haploid wild-type, *mto1Δ*, and dynein mutant cells in the presence of DMSO or MBC. Table S1 is a list of strains used in this study. Video 1 shows dynamics of microtubules and telomeres in cells undergoing cell conjugation. Video 2 shows dynamics of microtubules and telomeres in haploid meiotic cells after MBC removal. Video 3 shows microtubule nucleation from the vicinity of the telomere in haploid meiotic cells. Video 4 shows telomere and microtubule dynamics in a mitotic cell. Video 5 shows dynamics of microtubules and telomeres in haploid meiotic cells after MBC removal. Video 6 shows microtubule nucleation from telomere-localized Sad1 before cell conjugation. Online supplemental material is available at http://www.jcb.org/cgi/content/full/jcb.201207168/DC1.

We thank Y. Chikashige, T. Carr, J.R. McIntosh, J. Paluh, K. Sawin, K. Tanaka, T. Toda, A. Yamashita, M. Yamamoto, and the Yeast Genetic Resource Center for strains or reagents and J. Cooper, A. Shinohara, K. Tanaka, M. Uritani, and T. Ushimaru for critical reading of the manuscript and many helpful suggestions. We also thank K. Ichikawa for assisting live-cell observation.

This work was supported by Grants-in-aid for Scientific Research (C) and on Innovative Areas to A. Yamamoto and was performed in part under the Cooperative Research Program of the Institute for Protein Research, Osaka University.

Submitted: 27 July 2012
Accepted: 14 January 2013

## References

Bähler, J., J.Q. Wu, M.S. Longtine, N.G. Shah, A. McKenzie III, A.B. Steever, A. Wach, P. Philippsen, and J.R. Pringle. 1998. Heterologous modules for efficient and versatile PCR-based gene targeting in *Schizosaccharomyces pombe*. *Yeast*. 14:943–951. http://dx.doi.org/10.1002/(SICI)1097-0061(199807)14:10<943::AID-YEA292>3.0.CO;2-Y

Browning, H., J. Hayles, J. Mata, L. Aveline, P. Nurse, and J.R. McIntosh. 2000. Tea2p is a kinesin-like protein required to generate polarized growth in fission yeast. *J. Cell Biol.* 151:15–28. http://dx.doi.org/10.1083/jcb.151.1.15

Chikashige, Y., D.-Q. Ding, H. Funabiki, T. Haraguchi, S. Mashiko, M. Yanagida, and Y. Hiraoka. 1994. Telomere-led premeiotic chromosome movement in fission yeast. *Science*. 264:270–273. http://dx.doi.org/10.1126/science.8146661

Chikashige, Y., R. Kurokawa, T. Haraguchi, and Y. Hiraoka. 2004. Meiosis induced by inactivation of Pat1 kinase proceeds with aberrant nuclear positioning of centromeres in the fission yeast *Schizosaccharomyces pombe*. *Genes Cells*. 9:671–684. http://dx.doi.org/10.1111/j.1356-9597.2004.00760.x

Chikashige, Y., C. Tsutsumi, M. Yamane, K. Okamasa, T. Haraguchi, and Y. Hiraoka. 2006. Meiotic proteins bqt1 and bqt2 tether telomeres to form the bouquet arrangement of chromosomes. *Cell*. 125:59–69. http://dx.doi.org/10.1016/j.cell.2006.01.048

Cooper, J.P., E.R. Nimmo, R.C. Allshire, and T.R. Cech. 1997. Regulation of telomere length and function by a Myb-domain protein in fission yeast. *Nature*. 385:744–747. http://dx.doi.org/10.1038/385744a0

Ding, D.Q., A. Yamamoto, T. Haraguchi, and Y. Hiraoka. 2004. Dynamics of homologous chromosome pairing during meiotic prophase in fission yeast. *Dev. Cell*. 6:329–341. http://dx.doi.org/10.1016/S1534-5807(04)00059-0

Erent, M., D.R. Drummond, and R.A. Cross. 2012. *S. pombe* kinesins-8 promote both nucleation and catastrophe of microtubules. *PLoS ONE*. 7:e30738. http://dx.doi.org/10.1371/journal.pone.0030738

Grissom, P.M., T. Fiedler, E.L. Grishchuk, D. Nicastro, R.R. West, and J.R. McIntosh. 2009. Kinesin-8 from fission yeast: a heterodimeric, plus-end-directed motor that can couple microtubule depolymerization to cargo movement. *Mol. Biol. Cell*. 20:963–972. http://dx.doi.org/10.1091/mbc.E08-09-0979

Hagan, I., and M. Yanagida. 1992. Kinesin-related cut7 protein associates with mitotic and meiotic spindles in fission yeast. *Nature*. 356:74–76. http://dx.doi.org/10.1038/356074a0

Heald, R., R. Tournebize, T. Blank, R. Sandaltzopoulos, P. Becker, A. Hyman, and E. Karsenti. 1996. Self-organization of microtubules into bipolar spindles around artificial chromosomes in *Xenopus* egg extracts. *Nature*. 382:420–425. http://dx.doi.org/10.1038/382420a0

Hentges, P., B. Van Driessche, L. Tafforeau, J. Vandenhaute, and A.M. Carr. 2005. Three novel antibiotic marker cassettes for gene disruption and marker switching in *Schizosaccharomyces pombe*. *Yeast*. 22:1013–1019. http://dx.doi.org/10.1002/yea.1291

Hiraoka, Y., and A.F. Dernburg. 2009. The SUN rises on meiotic chromosome dynamics. *Dev. Cell*. 17:598–605. http://dx.doi.org/10.1016/j.devcel.2009.10.014

Krawchuk, M.D., and W.P. Wahls. 1999. High-efficiency gene targeting in *Schizosaccharomyces pombe* using a modular, PCR-based approach with long tracts of flanking homology. *Yeast*. 15:1419–1427. http://dx.doi.org/10.1002/(SICI)1097-0061(19990930)15:13<1419::AID-YEA466>3.0.CO;2-Q

Ligon, L.A., S.S. Shelly, M. Tokito, and E.L. Holzbaur. 2003. The microtubule plus-end proteins EB1 and dynactin have differential effects on microtubule polymerization. *Mol. Biol. Cell*. 14:1405–1417. http://dx.doi.org/10.1091/mbc.E02-03-0155

MacQueen, A.J., C.M. Phillips, N. Bhalla, P. Weiser, A.M. Villeneuve, and A.F. Dernburg. 2005. Chromosome sites play dual roles to establish homologous synapsis during meiosis in *C. elegans*. *Cell*. 123:1037–1050. http://dx.doi.org/10.1016/j.cell.2005.09.034

Maundrell, K. 1993. Thiamine-repressible expression vectors pREP and pRIP for fission yeast. *Gene*. 123:127–130. http://dx.doi.org/10.1016/0378-1119(93)90551-D

Miki, F., K. Okazaki, M. Shimanuki, A. Yamamoto, Y. Hiraoka, and O. Niwa. 2002. The 14-kDa dynein light chain-family protein Dlc1 is required for regular oscillatory nuclear movement and efficient recombination during meiotic prophase in fission yeast. *Mol. Biol. Cell*. 13:930–946. http://dx.doi.org/10.1091/mbc.01-11-0543

Miki, F., A. Kurabayashi, Y. Tange, K. Okazaki, M. Shimanuki, and O. Niwa. 2004. Two-hybrid search for proteins that interact with Sad1 and Kms1, two membrane-bound components of the spindle pole body in fission yeast. *Mol. Genet. Genomics*. 270:449–461. http://dx.doi.org/10.1007/s00438-003-0938-8

Mocz, G., and I.R. Gibbons. 2001. Model for the motor component of dynein heavy chain based on homology to the AAA family of oligomeric ATPases. *Structure*. 9:93–103. http://dx.doi.org/10.1016/S0969-2126(00)00557-8

Moreno, S., A. Klar, and P. Nurse. 1991. Molecular genetic analysis of fission yeast *Schizosaccharomyces pombe*. *Methods Enzymol.* 194:795–823. http://dx.doi.org/10.1016/0076-6879(91)94059-L

Niccoli, T., A. Yamashita, P. Nurse, and M. Yamamoto. 2004. The p150-Glued Ssm4p regulates microtubular dynamics and nuclear movement in fission yeast. *J. Cell Sci.* 117:5543–5556. http://dx.doi.org/10.1242/jcs.01475

Niwa, O., M. Shimanuki, and F. Miki. 2000. Telomere-led bouquet formation facilitates homologous chromosome pairing and restricts ectopic interaction in fission yeast meiosis. *EMBO J.* 19:3831–3840. http://dx.doi.org/10.1093/emboj/19.14.3831

Paluh, J.L., E. Nogales, B.R. Oakley, K. McDonald, A.L. Pidoux, and W.Z. Cande. 2000. A mutation in gamma-tubulin alters microtubule dynamics and organization and is synthetically lethal with the kinesin-like protein pkl1p. *Mol. Biol. Cell*. 11:1225–1239.

Penkner, A., L. Tang, M. Novatchkova, M. Ladurner, A. Fridkin, Y. Gruenbaum, D. Schweizer, J. Loidl, and V. Jantsch. 2007. The nuclear envelope protein Matefin/SUN-1 is required for homologous pairing in *C. elegans* meiosis. *Dev. Cell*. 12:873–885. http://dx.doi.org/10.1016/j.devcel.2007.05.004

Pidoux, A.L., M. LeDizet, and W.Z. Cande. 1996. Fission yeast pkl1 is a kinesin-related protein involved in mitotic spindle function. *Mol. Biol. Cell*. 7:1639–1655.

Ponticelli, A.S., and G.R. Smith. 1989. Meiotic recombination-deficient mutants of *Schizosaccharomyces pombe*. *Genetics*. 123:45–54.

Razafsky, D., and D. Hodzic. 2009. Bringing KASH under the SUN: the many faces of nucleo-cytoskeletal connections. *J. Cell Biol.* 186:461–472. http://dx.doi.org/10.1083/jcb.200906068

Rodriguez, A.S., J. Batac, A.N. Killilea, J. Filopei, D.R. Simeonov, I. Lin, and J.L. Paluh. 2008. Protein complexes at the microtubule organizing center regulate bipolar spindle assembly. *Cell Cycle*. 7:1246–1253. http://dx.doi.org/10.4161/cc.7.9.5808

Sachdev, P., S. Menon, D.B. Kastner, J.Z. Chuang, T.Y. Yeh, C. Conde, A. Caceres, C.H. Sung, and T.P. Sakmar. 2007. G protein beta gamma subunit interaction with the dynein light-chain component Tctex-1 regulates neurite outgrowth. *EMBO J.* 26:2621–2632. http://dx.doi.org/10.1038/sj.emboj.7601716

Sato, A., B. Isaac, C.M. Phillips, R. Rillo, P.M. Carlton, D.J. Wynne, R.A. Kasad, and A.F. Dernburg. 2009. Cytoskeletal forces span the nuclear envelope to coordinate meiotic chromosome pairing and synapsis. *Cell*. 139:907–919. http://dx.doi.org/10.1016/j.cell.2009.10.039

Sato, M., S. Dhut, and T. Toda. 2005. New drug-resistant cassettes for gene disruption and epitope tagging in *Schizosaccharomyces pombe*. *Yeast*. 22:583–591. http://dx.doi.org/10.1002/yea.1233

Sawin, K.E., P.C. Lourenco, and H.A. Snaith. 2004. Microtubule nucleation at non-spindle pole body microtubule-organizing centers requires fission yeast centrosomin-related protein mod20p. *Curr. Biol.* 14:763–775. http://dx.doi.org/10.1016/j.cub.2004.03.042

Scherthan, H. 2001. A bouquet makes ends meet. *Nat. Rev. Mol. Cell Biol.* 2:621–627. http://dx.doi.org/10.1038/35085086

Schroer, T.A. 2004. Dynactin. *Annu. Rev. Cell Dev. Biol.* 20:759–779. http://dx.doi.org/10.1146/annurev.cellbio.20.012103.094623

Schuh, M., and J. Ellenberg. 2007. Self-organization of MTOCs replaces centrosome function during acentrosomal spindle assembly in live mouse oocytes. *Cell*. 130:484–498. http://dx.doi.org/10.1016/j.cell.2007.06.025

Shaner, N.C., R.E. Campbell, P.A. Steinbach, B.N. Giepmans, A.E. Palmer, and R.Y. Tsien. 2004. Improved monomeric red, orange and yellow fluorescent proteins derived from *Discosoma* sp. red fluorescent protein. *Nat. Biotechnol.* 22:1567–1572. http://dx.doi.org/10.1038/nbt1037

Shimanuki, M., F. Miki, D.-Q. Ding, Y. Chikashige, Y. Hiraoka, T. Horio, and O. Niwa. 1997. A novel fission yeast gene, *kms1*$^{+}$, is required for the formation of meiotic prophase-specific nuclear architecture. *Mol. Gen. Genet.* 254:238–249. http://dx.doi.org/10.1007/s004380050412

Sikorski, R.S., and P. Hieter. 1989. A system of shuttle vectors and yeast host strains designed for efficient manipulation of DNA in *Saccharomyces cerevisiae*. *Genetics*. 122:19–27.

Starr, D.A., and J.A. Fischer. 2005. KASH 'n Karry: the KASH domain family of cargo-specific cytoskeletal adaptor proteins. *Bioessays*. 27:1136–1146. http://dx.doi.org/10.1002/bies.20312

Steinberg, G. 2007. Preparing the way: fungal motors in microtubule organization. *Trends Microbiol.* 15:14–21. http://dx.doi.org/10.1016/j.tim.2006.11.007

Tomita, K., and J.P. Cooper. 2007. The telomere bouquet controls the meiotic spindle. *Cell*. 130:113–126. http://dx.doi.org/10.1016/j.cell.2007.05.024

Tomlin, G.C., J.L. Morrell, and K.L. Gould. 2002. The spindle pole body protein Cdc11p links Sid4p to the fission yeast septation initiation network. *Mol. Biol. Cell*. 13:1203–1214. http://dx.doi.org/10.1091/mbc.01-09-0455

Troxell, C.L., M.A. Sweezy, R.R. West, K.D. Reed, B.D. Carson, A.L. Pidoux, W.Z. Cande, and J.R. McIntosh. 2001. *pkl1*$^{(+)}$and *klp2*$^{(+)}$: Two kinesins of the Kar3 subfamily in fission yeast perform different functions in both mitosis and meiosis. *Mol. Biol. Cell*. 12:3476–3488.

Vardy, L., and T. Toda. 2000. The fission yeast gamma-tubulin complex is required in $G_{(1)}$ phase and is a component of the spindle assembly checkpoint. *EMBO J.* 19:6098–6111. http://dx.doi.org/10.1093/emboj/19.22.6098

Venkatram, S., J.J. Tasto, A. Feoktistova, J.L. Jennings, A.J. Link, and K.L. Gould. 2004. Identification and characterization of two novel proteins affecting fission yeast gamma-tubulin complex function. *Mol. Biol. Cell*. 15:2287–2301. http://dx.doi.org/10.1091/mbc.E03-10-0728

West, R.R., E.V. Vaisberg, R. Ding, P. Nurse, and J.R. McIntosh. 1998. *cut11*$^{(+)}$: A gene required for cell cycle-dependent spindle pole body anchoring in the nuclear envelope and bipolar spindle formation in *Schizosaccharomyces pombe*. *Mol. Biol. Cell*. 9:2839–2855.

Yamamoto, A., and Y. Hiraoka. 2003. Monopolar spindle attachment of sister chromatids is ensured by two distinct mechanisms at the first meiotic division in fission yeast. *EMBO J.* 22:2284–2296. http://dx.doi.org/10.1093/emboj/cdg222

Yamamoto, A., R.R. West, J.R. McIntosh, and Y. Hiraoka. 1999. A cytoplasmic dynein heavy chain is required for oscillatory nuclear movement of meiotic prophase and efficient meiotic recombination in fission yeast. *J. Cell Biol.* 145:1233–1249. http://dx.doi.org/10.1083/jcb.145.6.1233

Yamamoto, A., K. Kitamura, D. Hihara, Y. Hirose, S. Katsuyama, and Y. Hiraoka. 2008. Spindle checkpoint activation at meiosis I advances anaphase II onset via meiosis-specific APC/C regulation. *J. Cell Biol.* 182:277–288. http://dx.doi.org/10.1083/jcb.200802053